Dissolved air flotation modelling: insights and shortcomings

Johannes Haarhoff and James K. Edzwald

ABSTRACT

The use of relatively simple but conceptually sound mathematical models is a powerful tool to identify and understand variables that affect the performance of a process. Such models have been used to better understand the many and complex dissolved air flotation (DAF) variables that are in play when water, flocs and air bubbles are mixed in the contact zone and then removed in the separation zone. The first purpose of this paper is to examine critically models that have been previously developed, primarily by the authors, for the contact and separation zones, and to summarize the insights gained from these efforts.

During the past 5–10 years, significant strides were made towards more efficient designs that allow reduced flocculation time and much higher hydraulic loading rates. These developments have also exposed some fundamental weaknesses in the traditional modelling approaches, as some systems are now working beyond the theoretical limits of feasibility. The second purpose of the paper, therefore, is to probe these weaknesses and to suggest some directions for future modelling efforts.

Key words | air bubbles, contact zone, dissolved air flotation, floc, models, separation zone

Johannes Haarhoff (corresponding author)
Rand Afrikaans University,
PO Box 524,
2006 Auckland Park,
South Africa
E-mail: *jh@ing.rau.ac.za*

James K. Edzwald
University of Massachusetts,
Amherst,
MA 01003,
USA

INTRODUCTION

The working of a dissolved air flotation (DAF) reactor is usually conceptualized as two distinctly different steps taking place in two distinctly different parts of the reactor, one following the other. In the first compartment, called the *contact* zone, previously flocculated particles are introduced together with a fine air bubble suspension, with the intention of forming floc–bubble aggregates. The suspension then moves to the second part of the reactor, called the *separation* zone, with the intention of collecting the aggregates in the float layer at the top of the tank, while collecting the clear subnatant at the bottom of the tank. Although there is no or only a partial physical barrier between these zones, a virtual *cross-flow* boundary is imagined. This type of thinking determined the modular structure of the empirical design parameters suggested in earlier literature (for example, Haarhoff & Van Vuuren 1993). It is implicitly assumed that flocs are pre-formed and do not grow any further in the DAF reactor; likewise that air bubbles retain their size once formed. Although bubble coalescence is recognized and studied as a significant phenomenon, it is generally seen as undesirable as it removes air from the 'useful' small bubble fraction (Haarhoff & Steinbach 1997*a*).

The modelling efforts up to now have followed this line of reasoning, with two types of models; one for each step. Some powerful insights have come from *contact zone modelling* (for example, Edzwald *et al.* 1990; Edzwald 1995), while *separation zone modelling* (for example, Haarhoff & Edzwald 2001) has provided additional illumination and understanding. The first part of the paper critically examines the previously developed models of these authors and summarizes their contributions towards an improved understanding of DAF.

After DAF had established itself as a viable, robust treatment technology for a variety of applications during

the 1970s and 1980s, the 1990s witnessed a rapid development of the process into loading and performance ranges never imagined before. A series of pilot studies (Edzwald *et al.* 1999; Amato *et al.* 2001) and full-scale applications (Kiuru 2000) demonstrated that DAF performs well at hydraulic loading rates which do not seem theoretically possible, thus exposing a number of potential flaws in the modelling approaches. The second part of the paper focuses on these discrepancies and suggests directions for improved modelling of the DAF process.

TYPICAL DESIGN AND OPERATIONAL PARAMETERS

The air bubble suspension

DAF is primarily distinguished from other phase separation processes by the introduction of an air suspension close to the point where the floc suspension enters the contact zone. The air suspension is defined usually as a *mass* concentration C_b, ranging from 6 to 12 mg l^{-1}. The suspension consists of microbubbles, with an average bubble diameter d_b of 40–80 μm. For modelling purposes, it is convenient to visualize discrete air bubbles that are described better by their *number* concentration n_b or their *volume* concentration ϕ_b. The relationships are:

$$n_b = \left(\frac{C_b}{\rho_b}\right)\left(\frac{6}{\pi {d_b}^3}\right) \quad (1)$$

$$\phi_b = \frac{C_b}{\rho_b} \quad (2)$$

For average bubble size of about 60 μm, the typical number concentration of air bubbles is thus between 44 and 88×10^6 bubbles l^{-1} and the typical volume concentration is between 5,000 and 10,000 ppm. If these bubbles were evenly spaced the separation distance between bubbles would range from 160 to 220 μm.

The air mass concentration can be directly measured within a reasonably narrow confidence interval (see Haarhoff & Steinbach 1997*b* for a review of measurement methods and a recommended standard procedure). The average bubble diameter is difficult to measure, but the literature contains some measured and assumed sizes. Schers & Van Dijk (1992) and Liers *et al.* (1996), for example, assumed average bubble diameters of 30 to 40 μm to make similar calculations to those in the previous paragraph. Han *et al.* (2002) used image analysis and a particle counter, and found a mean bubble size immediately after formation, for a saturation pressure of 600 kPa, for the two methods, of 32 and 28 μm, respectively. The most comprehensive study on bubble size known to the authors is the work performed by Rykaart (1994). In his study, he performed 85 different experiments with a wide variety of nozzle types, during which more than 16,000 air bubbles were photographed, measured and counted with image analysis. All experiments were conducted at a saturation pressure of either 200 kPa or 500 kPa. At 200 kPa, the average bubble size was 82 μm with standard deviation of 22 μm; at 500 kPa the average bubble size was 62 μm with standard deviation of 22 μm. (The percentage of bubbles larger than 150 μm, incidentally, was 7.7% and 3.4%, respectively.) As most DAF systems operate at or close to 500 kPa, an average bubble size of 60 μm is used for the modelling examples in this paper.

The floc suspension

The floc suspension is easily characterized by its *mass* concentration C_f, which is made up of raw water particles and particles produced by the water treatment chemicals added. Although DAF is an efficient phase separation process for floc suspensions up to 100 mg l^{-1}, the typical floc mass concentration varies between 5 and 50 mg l^{-1}. For high quality reservoirs and lakes of low to moderate alkalinity as found in many areas of the United States, Finland and other places, the floc mass concentration would most likely be less than 10 mg l^{-1}. For other supplies, the raw water particle mass concentration could be 25 mg l^{-1} with another 25 mg l^{-1} typically added through coagulant addition. For modelling purposes, however, it is necessary to deal with the *number* concentration n_f of the flocs and their average diameter d_f. To make this conversion, an average floc density ρ_f is assumed (as for example by Baeyens *et al.* 1995). When a broad range of

floc sizes is considered, as in this paper, it is prudent to estimate the floc density by means of an appropriate fractal dimension D_{fr}, which leads to lower density as the floc size increases, a fact well supported by practical observation. There is consensus that flocs have a fractal, self-similar structure (possibly with different fractal dimensions over different size ranges). Theoretically, the range is from $D_{fr}=1$ (the minimum where structures are perfectly linear) to $D_{fr}=3$ (the theoretical maximum where structures are perfect solids).

The effective floc density is a function of floc size and is conveniently described in terms of the floc fractal dimension:

$$\rho_f-\rho_w \propto d_f^{D_{fr}-3} \tag{3}$$

For flocs with size d_f composed of primary particles with size d_p and density ρ_p, the density is obtained by successive application of Equation (3) to flocs and primary particles:

$$\rho_f=\rho_w+(\rho_p-\rho_w)\left(\frac{d_f}{d_p}\right)^{D_{fr}-3} \tag{4}$$

A summary of experimentally measured fractal dimensions of the aggregates found in water treatment (Wiesner 1992) covers an extremely wide range from $D_{fr}=1.3$ to 2.8. The very wide range is partially explained by the choice of floc size definition (Adachi & Tanaka 1997), the fluid mechanical environment in which the flocs are formed (Logan & Kilps 1995) and probably by differences in experimental procedure. Further insight comes from theoretical and computer simulations, which indicate an upper boundary of $D_{fr}=2.75$ for interactions between single primary particles and clusters (diffusion-limited aggregation) and a lower boundary of $D_{fr}=1.75$ for cluster–cluster interaction (Gregory 1989). Other studies (summarized by Jiang & Logan 1991) show that the fractal dimension is determined by the dominant transport mechanism, as well as the collision efficiency or sticking factor, α. Floc formation by Brownian motion leads to fractal dimensions 1.8–2.2; the lower number by high collision efficiency and the higher number by poor collision efficiency, where primary particles penetrate deeper into the floc before eventually sticking. Differential sedimentation leads to fractal dimensions of 1.6–2.3, while floc formation by fluid shear (velocity gradients from mixing) leads to fractal dimensions of 2.4 or more. The fractal dimensions of inorganic aggregates (typical of water treatment) are higher than those of organic aggregates formed in activated sludge or in the ocean as marine snow.

From the above references, the fractal dimensions of water treatment flocs generally seem to converge on a range of about $D_{fr}=1.8$ ('open' flocs which do not settle readily) to $D_{fr}=2.4$ ('compact' flocs which settle more readily). In this paper, the authors use fractal dimensions in the upper end of the reported range; a choice guided by the fact that full-scale systems are usually reasonably efficient. These values are $D_{fr}=2.1$ (to illustrate poorer floc settling) and $D_{fr}=2.3$ (to illustrate better floc settling).

The nature of the primary particles in the raw water is highly variable. To illustrate, primary kaolin particles with sizes of 0.3–3 μm and density 2,650 kg m^{-3} are assumed and compared with primary algae particles of 10 μm and density 1,020 kg m^{-3}. Kaolin is a well-known laboratory test suspension with fractal self-similarity of the flocs formed when coagulated by aluminium sulphate (Adachi & Tanaka 1997). As both the contact and separation zones will be modelled, a wide range of floc sizes is considered.

With a floc mass concentration of C_f, the floc number concentration n_f is calculated for any floc size d_f:

$$n_f=\left[\rho_w+(\rho_p-\rho_w)\left(\frac{d_f}{d_p}\right)^{D_{fr}-3}\right]^{-1}\frac{6C}{\pi d_f^3} \tag{5}$$

With the floc number concentration known, the separation distance between perfectly spaced flocs can be determined. Table 1 provides such estimates for finely dispersed clay, coarser clay and a typical algal suspension. A number of conclusions follow from Table 1:

- For large flocs, the density of the primary particles plays a relatively minor role.
- The density of algal flocs remains very close to that of water, regardless of the floc size or the fractal dimension.
- The separation distance between flocs is many times more than the typical DAF bubble sizes.

Table 1 | Typical floc properties for different fractal dimensions (conditions: C_f=10 mg l^{-1}; only properties of primary particles considered, flocs distributed evenly throughout the sample)

Fractal dimension		2.1			2.3	
Floc diameter (μm)	10	100	500	10	100	500
Clay						
$d_p = 0.3$ μm						
$\rho_p = 2{,}650$ kg m^{-3}						
ρ_f (kg m^{-3})	1,070	1,009	1,002	1,142	1,028	1,009
Separation distance (μm)	373	2,652	18,218	381	3,676	18,262
Clay						
$d_p = 3$ μm						
$\rho_p = 2{,}650$ kg m^{-3}						
ρ_f (kg m^{-3})	1,558	1,070	1,017	1,710	1,142	1,046
Separation distance (μm)	424	3,727	18,308	437	3,810	18,488
Algae						
$d_p = 10$ μm						
$\rho_p = 1{,}020$ kg m^{-3}						
ρ_f in kg m^{-3}	–	1,003	1,001	–	1,004	1,001
Separation distance in μm	–	3,644	18,209	–	3,646	18,214

Flocculation time

When DAF was first applied to drinking water treatment, the flocculation tanks prior to DAF were designed similar to flocculation tanks preceding settling. Hence, flocculation times were about 20–30 min. Since then, flocculation times have been systematically reduced (a point discussed in more detail later in the paper) to current design guidelines which indicate that flocculation times as low as 5–10 min are suitable for drinking water DAF plants.

Contact zone geometry

A survey of six Dutch plants (Schers & Van Dijk 1992) indicated a range of contact zone detention times of 0.9–2.1 min, with a median of 1.7 min. A design guideline suggested a detention time of 1–4 min (Haarhoff & Van Vuuren 1993), and Baeyens *et al.* (1995) suggested an average detention time of 1.5–2.5 min. Other recommendations regarding the contact zone geometry were a hydraulic loading 40–100 m h^{-1}, a contact zone depth 1.5–3.0 m (usually the same as the separation zone depth) and a cross-flow velocity (calculated as the average velocity over the virtual plane between the contact and separation zones) 20–100 m h^{-1} (Haarhoff & Van Vuuren 1993).

Separation zone geometry

The hydraulic loading is the primary design parameter of the separation zone. It is usually calculated from the entire

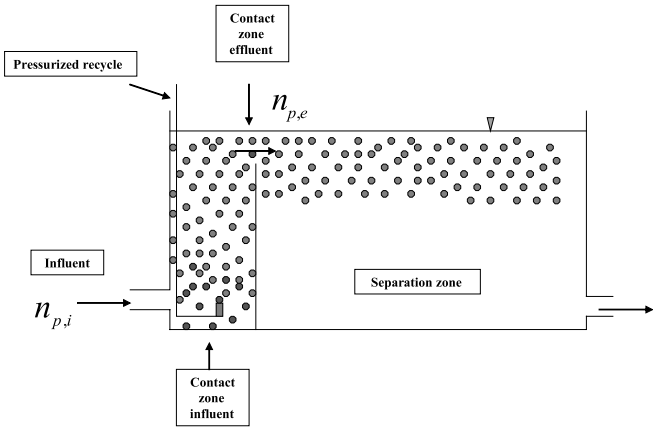

Figure 1 | Schematic of a DAF tank showing a blanket of air bubbles in the baffled section of the contact zone extending into the top part of the separation zone.

footprint of the DAF reactor (both contact and separation zones), but in the interest of clarity it should be calculated from the separation zone footprint only, as is done in this paper. As in the case of flocculation time, designs in the past were conservative at about 5 m h^{-1}. With time, the hydraulic loadings were systematically increased to values as high, recently, as 40 m h^{-1}. This evolution of loading rates, and its implications, is the topic of a later section of this paper. Due to this broad variation in hydraulic loading, the average detention time in the separation zone covers the wide range of 2–36 min.

CONTACT ZONE MODELLING

The DAF tank as shown in Figure 1 is divided into two zones. The contact zone, from a design view, is depicted functionally to reside on the left-hand side of the baffle. The contact zone model initially developed by Edzwald and co-workers (Edzwald *et al.* 1990; Malley & Edzwald 1991; Edzwald 1995) is summarized and discussed. The modelling approach considers bubbles in the *white water* blanket of air bubbles within the contact zone as collectors of particles using the single collector collision efficiency approach to account for particle transport collisions with bubbles. The model is developed by considering this blanket of air bubbles to exist in the contact zone at a dynamic steady state at high bubble concentration ($n_b > 10^7$ bubbles l^{-1}), which is continuously regenerated with air bubbles from injection of recycle from the saturator and removal of bubbles and floc–bubble aggregates at the cross-flow plane to the separation zone. In the development of the model below, the term particle is used in a general sense and refers to primary particles that enter the flotation tank or to flocculated particles.

The kinetic rate of particle or floc (n_p) removal by collision and attachment to bubbles is

$$\frac{dn_p}{dt} = -k_c n_p \tag{6}$$

where, k_c is the DAF rate coefficient dependent on the mass transport of particles to bubble surfaces and on the particle–bubble attachment efficiency (α_{pb}). Using the single collector collision efficiency (η_T) to account for particle transport, the rate coefficient depends upon:

$$k_e = \alpha_{pb}\eta_T v_b A_b n_b \tag{7}$$

The projected area of the bubble (A_b) is replaced by ($\pi d_b^2/4$), and the bubble number concentration (n_b) is replaced with the bubble volume concentration (ϕ_b) using Equations (1) and (2). Equations (6) and (7) are then incorporated into a steady state mass balance for plug flow conditions in the contact zone yielding the following *white water* model performance equation.

$$\left(1 - \frac{n_{p,e}}{n_{p,i}}\right) = \left[1 - exp\left(\frac{-\frac{3}{2}\alpha_{pb}\eta_T \phi_b v_b t_{cz}}{d_b}\right)\right] \tag{8}$$

This equation describes the efficiency for removal of particles or flocs on to bubbles within the contact zone. The dimensionless particle transport coefficient (η_T) describes the collision efficiency of a single bubble or collector. Collisions due to particle transport from the bulk water are considered to occur through four mechanisms: Brownian diffusion (η_D), fluid flow or interception (η_I), differential settling of flocs (η_S) and inertia (η_{IN}).

Equations (9) through (12) describe these individual collision efficiencies.

$$\eta_D = 6.18\left[\frac{k_b T}{g(\rho_w - \rho_b)}\right]^{2/3}\left[\frac{1}{d_p}\right]^{2/3}\left[\frac{1}{d_b}\right]^{2} \quad (9)$$

$$\eta_1 = \left(\frac{d_p}{d_b}+1\right)^2 - \frac{3}{2}\left(\frac{d_p}{d_b}+1\right) + \frac{1}{2}\left(\frac{d_p}{d_b}+1\right)^{-1} \quad (10)$$

$$\eta_s = \left[\frac{(\rho_p - \rho_w)}{(\rho_w - \rho_b)}\right]\left[\frac{d_p}{d_b}\right]^2 \quad (11)$$

$$\eta_{IN} = \frac{g\rho_p\rho_w d_b (d_p)^2}{324(\mu_w)^2} \quad (12)$$

Equation (10) is the general solution for interception of particles by bubbles as derived from particle trajectory analysis (Yu 1989). It can be shown for the case of $d_p/d_b \ll 1$ that Equation (10) gives the same result as an approximate expression of $\eta_I = 3/2(d_p/d_b)^2$. Equation (10) should be used for DAF modelling because the approximate expression does not hold for floc particles (d_p) of 10s of microns and bubbles (d_b) of, say, 60 μm. Earlier publications by Edzwald mistakenly show the approximate equation for interception. η_I calculations using the approximate expression for floc particles of 10–60 μm yield values 1.05 to 1.2 times too large. Thus, the general equation should be used for single collector efficiency calculations. On the other hand because of the influence of the other variables, especially the large number of collectors, the effect of using the approximation for η_I on the contact zone performance model (Equation (8)) is small. Nonetheless, Equation (10) is used in this paper. A general solution equivalent to Equation (10) was derived by Yao (1968) for water filtration, but of course the approximation applies because filter media collectors are much larger than floc particles.

The total single collector collision efficiency (η_T) is the sum of the individual mechanisms:

$$\eta_T = \eta_D + \eta_I + \eta_S + \eta_{IN} \quad (13)$$

The last term in Equation (13) describing collisions by inertial transport is not significant for bubbles and flocs less than 100 μm.

For particles to be removed in flotation, they must attach or stick to air bubbles on collision. In the contact zone efficiency model (Equation (8)), this is accounted for by an empirical factor α_{pb}. It is assigned values ranging from near zero (poor attachment) to 1 (all collisions lead to attachment). It is possible to make theoretical calculations of α_{pb} (Han 2000) based on short-range electrostatic interactions and Van der Waals forces. These theoretical calculations require measurements of electrical charge potentials of flocs and bubbles and values for the Hamaker constant. The empirical evaluation of α_{pb} is preferred by the authors, given the heterodispersed nature of particles in water supplies, their charge properties, the effect of natural organic matter on charge, and changes that occur through coagulation. Additional reasons for this approach follow.

First, this empirical assignment has been widely used to evaluate particle attachment or sticking in flocculation and filtration modelling. Second, it is used conceptually to reflect the chemistry of the system in terms of how coagulation makes the particles or flocs sticky with respect to attachment to bubbles. Finally, it allows one to view particle or floc removal by air bubbles in the contact zone as a two-step process: particle transport and particle attachment. Our modelling approach effectively makes α_{pb} a variable that depends on the coagulation chemistry. This is not entirely the case since we ignore hydrodynamic retardation in evaluation of η_T. Some researchers attempt to include the short-range forces of electrostatic interactions, Van der Waals forces, and hydrodynamic retardation in particle trajectory analysis in equations for η_T (see Derjaguin *et al.* 1984; Leppinen 2000). The modelling approach used here incorporates these effects into the empirical factor, α_{pb}.

Particle or floc properties and water temperature

First, the effects of α_{pb} (particle–bubble attachment factor) and particle or floc size on the contact zone efficiency are addressed. This is followed by examination of the effect of particle density and, finally, the effect of water temperature. In this section, certain model parameters are fixed. They are the bubble size (d_b) at 60 μm, bubble volume

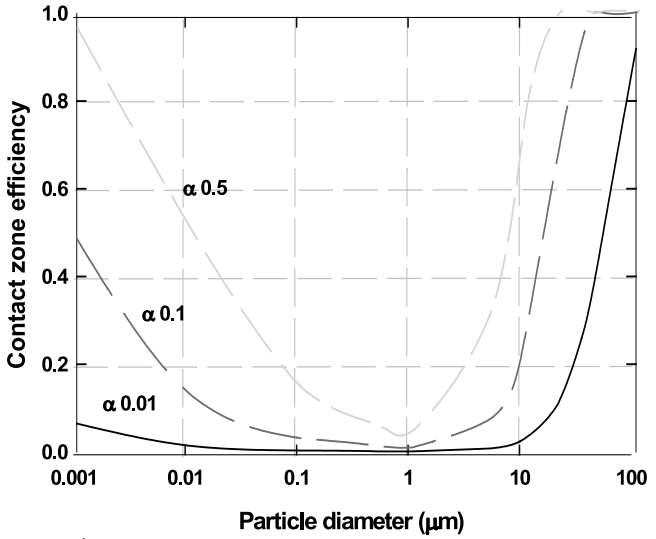

Figure 2 | Effect of the particle–bubble attachment factor (α_{pb}) on the contact zone efficiency as a function of particle or floc size (conditions: t_{cz}=3 min, T=293 K, ρ_p=1,100 kg m^{-3}, d_b=60 μm, and ϕ_b=8,000 ppm).

concentration (ϕ_b) at 8,000 ppm, and the contact zone detention time (t_{cz}) at 3 min. The selected values are typical for DAF; their variation is examined in the subsequent section.

Favourable attachment (high α_{pb} values) of particles to bubbles requires reduction in charge interaction between particles and bubbles so that Van der Waals forces can prevail. Coagulant chemicals are used to obtain favourable attachment so α_{pb} depends on coagulation conditions (type, dosage and pH). In some waters hydrophilic colloids may exist that are resistant to bubble attachment, but proper coagulation can alter the colloid surface properties so that attachment to bubbles is favoured.

Contact zone model predictions are presented in Figure 2 for three assigned α_{pb} values: 0.01 (no coagulation pre-treatment), 0.1 (poor coagulation) and 0.5 (good coagulation). Without coagulation (α_{pb} of 0.01 or less), the contact zone efficiency is poor for all particle or floc sizes except for very large flocs. With coagulation there is considerable improvement in the contact zone efficiency for small flocs. It is important, however, to optimize coagulation (illustrated here as α_{pb} of 0.5) as opposed to non-optimum or poor coagulation (α_{pb} of 0.1). Figure 2 shows that, for a floc size of only 10 μm, the contact zone efficiency is 80% for optimum coagulation conditions compared with <30% for poor coagulation.

The effect of particle size on the contact zone efficiency is greatly influenced by particle mass transport through Equations (9)–(11). Particle transport by Brownian diffusion is the controlling mechanism for particles <1 μm while transport by interception controls for particles or flocs >1 μm; transport by settling of flocs on to bubbles is not significant for low-density floc. The model predictions in Figure 2 show that there is a minimum in the contact zone efficiency for particles of about 1 μm. This size should be avoided. This minimum in contact zone efficiency for 1 μm particles is analogous to granular media filtration, in which there is also a minimum in filtration efficiency for the same particle size. This is because the physics of particle transport is the same for the two processes.

The effect of particle size on contact zone efficiency is examined in more detail for good coagulation or favourable attachment conditions of α_{pb} equal to 0.5. Flocculation tanks change the size distribution of particles and prepare flocs for effective removal by flotation. Figure 2 shows that flocculation tanks should be designed to produce flocs of 10s of microns for the influent to DAF tanks. Flocs of 10s of microns have high η_T values and thus yield good contact zone removal efficiencies; for example, floc sizes of 10 and 20 μm yield contact zone efficiencies of 80% and 99%. While increasing flocs to larger sizes theoretically increases η_T and the contact zone efficiency, large floc size is not necessary to yield high efficiencies. Furthermore, large flocs require multiple bubble attachment to lower floc–bubble aggregate density and to prevent detachment of floc particles.

The model calculations presented above were made for particles or flocs in the contact zone with a density of 1,100 kg m^{-3}. Figure 3 compares contact zone efficiencies for two floc densities: 1,100 and 2,500 kg m^{-3}. High floc density increases the single collector efficiency for sedimentation (transport of flocs to bubbles by settling, η_S, Equation (11)), but the predictions in Figure 3 show that particle transport by interception is far more important than particle transport by sedimentation since there is a very small effect of particle density on the contact zone efficiency.

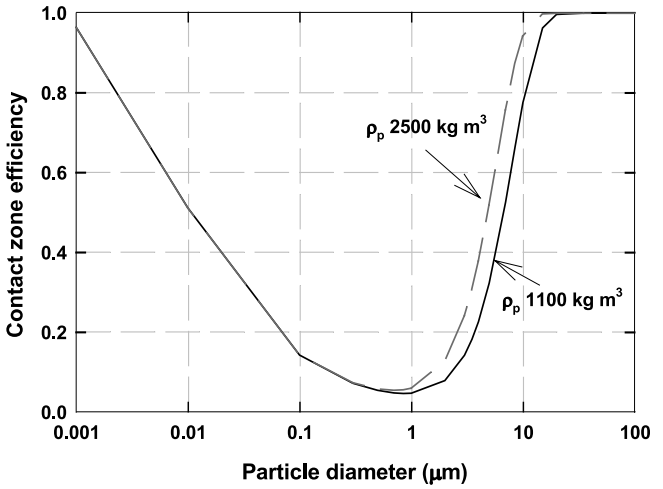

Figure 3 | Effect of the particle or floc density (ρ_p) on the contact zone efficiency as a function of particle or floc size (conditions: t_{cz}=3 min, T=293 K, α_{pb}=0.5, d_b=60 μm, and ϕ_b=8,000 ppm).

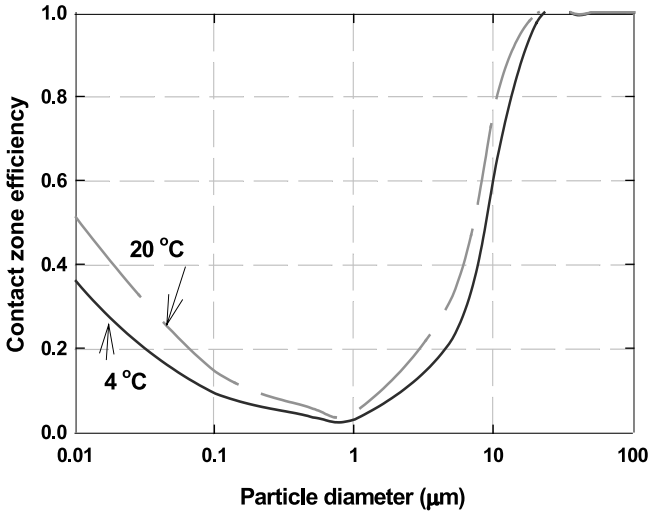

Figure 4 | Effect of water temperature on the contact zone efficiency as a function of particle or floc size (conditions: t_{cz}=3 min, α_{pb}=0.5, ρ_p=1,100 kg m^{-3}, d_b=60 μm, and ϕ_b=8,000 ppm).

The effect of water temperature on the contact zone efficiency is examined in Figure 4. Decreasing water temperature reduces the single collector efficiency by Brownian diffusion for small particles but the effect is small (Equation (9)). Cold water also decreases the bubble rise velocity, which will reduce the contact zone efficiency (Equation (8)). However, the overall impact of decreasing water temperature on the efficiency can be small for flocs,

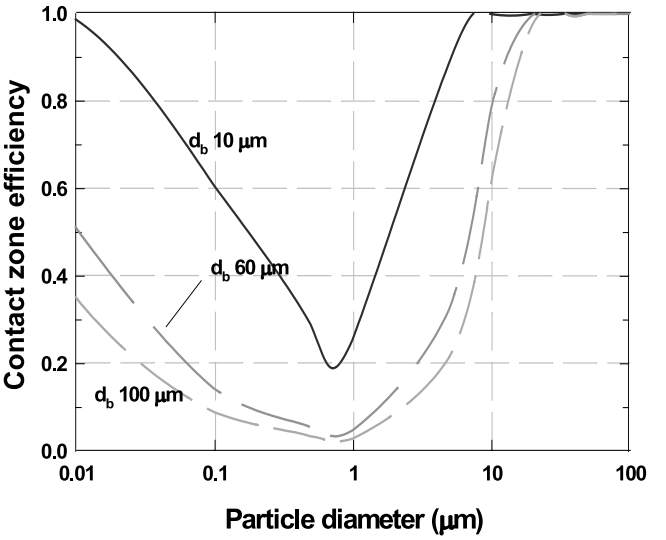

Figure 5 | Effect of bubble diameter on contact zone efficiency as a function of particle or floc size (conditions: t_{cz}=3 min, T=293 K, α_{pb}=0.5, ρ_p=1,100 kg m^{-3}, and ϕ_b=8,000 ppm).

as illustrated in Figure 4. For low density flocs with size >1 μm, interception is the important mechanism so that temperature only impacts the bubble rise velocity and the effect is small; for example, a 10 μm floc has a contact zone efficiency of 80% in warm water (20°C) which decreases to 60% in cold water (4°C), while the efficiencies for a 20 μm floc are hardly affected: 99 and 98% for warm and cold waters.

Bubble size and bubble volume concentration

A distinctive feature of DAF is the *white water* blanket that is formed in the contact zone due to the presence of microbubbles in the 10–100 μm size range. Overall, the contact zone efficiency depends on the inverse of the bubble diameter as shown in Equation (8). Contact zone model predictions for bubble diameters of 10, 60 and 100 μm are presented in Figure 5. Particle collection efficiency improves with decreasing bubble size for all particle or floc sizes. Considering the efficiency of 60 μm compared with 100 μm bubbles for flocs of 10 μm, one can see from Figure 5 that the contact zone efficiency increases from 60% for 100 μm bubbles to 80% for 60 μm bubbles. These model predictions agree with observations

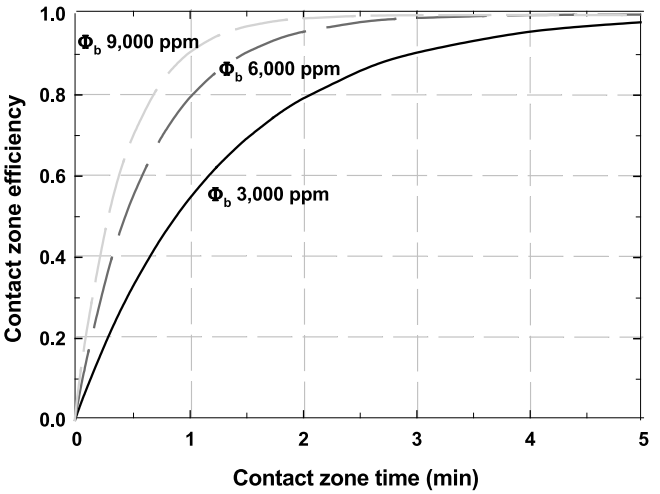

Figure 6 | Effect of bubble volume concentration on the contact zone efficiency as a function of contact zone time for 20 μm flocs (conditions: T=293 K, α_{pb}=0.5, ρ_p=1,100 kg m^{-3}, and d_b=60 μm).

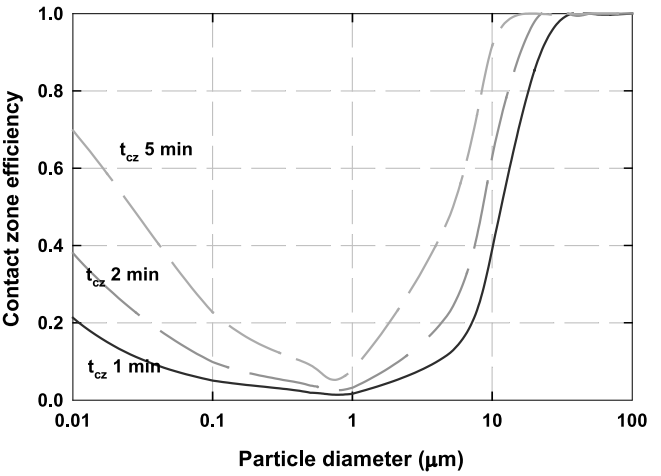

Figure 7 | Effect of contact zone time on contact zone efficiency as function of particle or floc size (conditions: T=293 K, α_{pb}=0.5, ρ_p=1,100 kg m^{-3}, d_b=60 μm, and ϕ_b=8,000 ppm).

that small bubble flotation processes such as DAF are more efficient than processes with larger size bubbles such as dispersed air flotation.

The average bubble size is controlled principally by the pressure difference across the injection device and also by the injection device (nozzle design). There is a diminishing return on bubble size by increasing the saturator pressure above 500 kPa; thus most new saturators utilize packing to increase the transfer efficiency and operate at 400–500 kPa. While there is not much control of the average bubble *size* in design and operation, the bubble *concentration* is controlled by the recycle rate and is an important variable. The wide range of bubble sizes considered in Figure 5 was chosen to account for the often wide distribution of bubble sizes about the average bubble size.

Figure 6 shows the effect of bubble volume concentration on the contact zone efficiency for removing 20 μm flocs as a function of the contact zone detention time. Contact zone design times are in the range of 1–5 min and are, typically, 2–4 min. Poor efficiency occurs for low bubble volume concentrations (3,000 ppm, mass concentration of 3.6 mg l^{-1}) unless high detention times are used. DAF systems are usually designed to release about 10 mg l^{-1} (bubble volume concentration of 8,400 ppm). At these bubble volume concentrations, as illustrated in Figure 6 with the predictions for 6,000 to 9,000 ppm, the contact zone efficiency is rather insensitive to detention time for contact times exceeding 1.5 min. The model calculations agree with design practices. The model calculations also show that DAF tanks need a contact zone detention time of at least 1 min as efficiency decreases significantly for shorter times.

Figure 7 addresses contact zone efficiency as a function of particle or floc size for three contact zone detention times (1, 2 and 5 min). These calculations were made for a bubble concentration of 8,000 ppm, typical of design conditions. The model results show a minimum in efficiency for about 1 μm particles or flocs. Furthermore, they show poor removals for particles less than 1 μm except for high contact times. The calculations reinforce the need to form floc sizes of 10s of microns. Contact zone efficiencies for 10 μm flocs range from about 40 to 90% for corresponding contact zone times of 1–5 min, but increase to 90% or greater for 20 μm flocs.

Contact zone model confirmation

Experimental pilot-scale DAF plant data were collected to test the contact zone model. The pilot plant had a flow rate

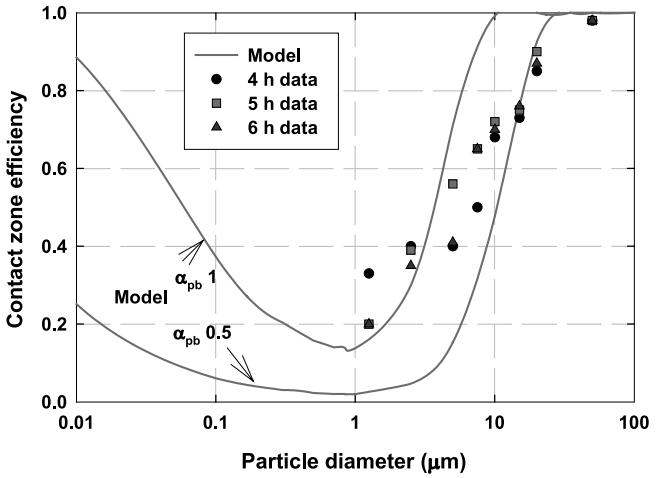

Figure 8 | Model versus experimental data (model assumptions: d_b=60 μm and α_{pb} of 0.5 and 1; experimental conditions: DAF loading rate 15 m h^{-1}, t_{cz}=1.9 min, T=278.5 K, Φ_b=7,840 ppm).

of 20 m^3 h^{-1} and consisted of static mixers for coagulation addition, two stage flocculation (total detention time of 5 min), and DAF at a gross hydraulic loading of 15 m h^{-1}. The DAF recycle rate was 8% with a saturator pressure of 550 kPa. The raw water was a reservoir supply with the following conditions: temperature 5.5°C, turbidity 0.7 NTU and particle counts 6,000 particles ml^{-1} (1–200 μm; most particles <20 μm; a research grade light, blockage type counter was used). A dual coagulant strategy of alum and a cationic polymer was used with alum at 1.5 mg l^{-1} as Al and cationic polymer dose of 1 mg l^{-1} (liquid product). This coagulant strategy is used by a full-scale plant at the same site and produces flocs with charge near zero. The pH after coagulation was 6.7–6.8. These coagulation conditions are considered favourable for good floc–bubble attachment.

The model was tested by making particle size distribution measurements after flocculation (DAF contact zone influent) and at the top of the baffle of the contact zone (DAF contact zone effluent). The DAF bubble volume concentration was estimated at 7,840 ppm. A bubble size of 60 μm was assumed, based on the motivation provided earlier. Floc particle concentrations in the influent and effluent of the contact zone were measured at 4, 5 and 6 h into the experimental test. Figure 8 compares the model predictions (curves) for two assumed alpha values (α_{pb} of 0.5 and 1) against the experimental data. The experimental data are fairly constant with time indicating steady state performance, an assumption of the model (Equation (8)). There is reasonable agreement between the model and experimental data with poor floc removals occurring for sizes near 1 μm and good performance for sizes of 10s of microns. For floc sizes of 1–5 μm, the model prediction agrees with the data if an α_{pb} of 1 is assumed. For larger floc sizes, the experimental data lie within model predictions assuming α_{pb} between 0.5 and 1. These assigned α_{pb} values of 0.5–1 adequately model the data and agree reasonably well with α_{pb} values in the literature using our contact zone model.

Schers & Van Dijk (1992) found α_{pb} of 0.2–1 for six Dutch DAF water plants, while Shawwa and Smith (1998) reported experimentally determined α_{pb} values of 0.35–0.55 for optimum coagulation conditions for an algal suspension. The model and field data show that the contact zone efficiency for small floc particles of 10–30 μm in drinking water treatment is very efficient. In some flotation applications (industrial or municipal wastewaters), large particles and flocs may pre-exist, but that is not the case for most drinking water applications where colloidal particles are dominant in source waters, especially reservoir supplies. Furthermore, removal of natural colour and dissolved natural organic matter involves a phase change in which particles are produced following coagulant addition.

SEPARATION ZONE MODELLING

To predict the rise rate of a floc–bubble aggregate, it is necessary to first derive an expression for the settling rate of a floc on its own, before bubbles are mathematically 'added' to the floc. The floc settling rate is modelled here by modifying the familiar Stokes' equation for solid spheres, an approach questioned because of its neglect of the following refinements (Johnson *et al.* 1996):

- The floc is not impermeable, allowing some water to flow through the floc. The assumption of a solid floc therefore slightly underestimates the settling velocity.

- The drag coefficient is also a function of the fractal dimension, as the uneven distribution of voids within the floc allows more flow-through than with evenly distributed primary particles. The conventional assumption of a drag coefficient being a function of floc shape and Reynolds number only, therefore also underestimates the settling velocity.

In this paper, the goal is to eventually obtain an estimate of the rise rate of a floc–bubble aggregate which is many times more than the settling rate of a floc, and driven by much larger buoyancy forces. The authors have therefore opted for the simplified derivation below, as it is sufficient to illustrate the desired points.

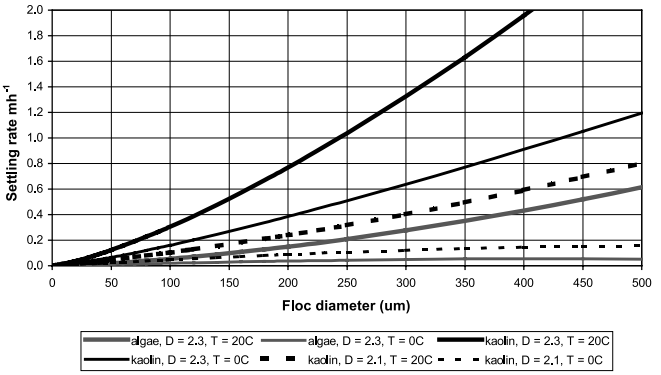

Figure 9 | Calculated floc settling rates for different suspension types, temperatures and fractal dimensions (conditions for kaolin: d_p=0.3 μm, ρ_p=2,650 kg m^{-3}; conditions for algae: d_p=10 μm, ρ_p=1,020 kg m^{-3}).

Theoretical settling rate of a floc

The general expression for the settling rate of a particle in water, derived from a balance between shear and gravitational forces, is:

$$v_p = \sqrt{\frac{4g(\rho_p - \rho_w)d_p}{3C_D\rho_w}} \tag{14}$$

Laminar flow conditions prevail if the Reynolds number is less than unity:

$$Re = \frac{v_p d_p \rho_w}{\mu_w} < 1 \tag{15}$$

The Reynolds number is assumed to be below unity for floc settling in water treatment. For these laminar conditions, the drag coefficient can be expressed as:

$$C_D = \frac{K}{Re} = \frac{K\mu_w}{v_p d_p \rho_w} \tag{16}$$

Substitution of Equation (16) into Equation (14) leads to the following formulation of Stokes' Law:

$$v_p = \frac{4g(\rho_s - \rho_w){d_p}^2}{3K\mu_w} \tag{17}$$

For perfect spheres, $K = 24$. For floc particles with a sphericity of 0.8, Tambo & Watanabe (1979) suggested a value of $K = 45$. Using this value in Equation (17), we find that the settling rate of flocs is about half that of perfect spheres:

$$v_f = \frac{4g(\rho_f - \rho_w){d_f}^2}{135\mu_w} \tag{18}$$

Substitution of the density term by Equation (4) to reflect the fractal nature of the flocs leaves an expression for the settling rate in terms of the fractal dimension and the properties of the primary particles. It was used to develop Figure 9, which demonstrates the simplified settling model above for kaolin and algae, neglecting the additional presence of particles formed by the coagulant, at different fractal dimensions and water temperatures. From the trends, rather than the absolute value of the settling velocity, a number of conclusions become evident:

- The settling velocity increases relatively slowly with increasing floc size. To improve the settling of a suspension would therefore require a substantial increase in floc size.
- Low-density particles, even when grown to very large flocs, do not reach settling rates which are practically acceptable, necessitating the use of DAF or other technologies.

- The well-known effect of temperature is clearly demonstrated, effectively reducing the settling rate by 50% as the temperature drops from 20°C to 0°C.
- The density of the floc structure, as reflected here by a relatively small difference in fractal dimension, has a huge effect on settling rate, even larger than temperature in this specific example.

Theoretical rise rate of a floc–bubble aggregate

The equations developed in the previous section can be adapted to predict the rise rates of floc–bubble aggregates or, simply, aggregates. The aggregate equivalent diameter d_{fb} produced from N bubbles of size d_b adhering to a single floc particle with size d_f is estimated by assuming that the bubble and floc volumes are additive:

$$d_{fb} = (d_f^3 + N d_b^3)^{1/3} \tag{19}$$

Its density ρ_{fb} is estimated from the weighted average of the air and floc densities:

$$p_{fb} = \frac{\rho_f d_f^3 + N \rho_b d^3 b}{d^3{}_f + N d_b^3} \tag{20}$$

Once the aggregate size and density are found, a rise rate equation is developed similar to the settling equation in the previous section. The density terms in Equation (17) are reversed to obtain a positive rise rate:

$$v_{fb} = \frac{4g(\rho_w - \rho_{fb}) d_{fb}^2}{3K\mu_w} \tag{21}$$

In this case, K is not constant for all sizes. For the case of a small floc of 5 μm attached to a bubble of 50 μm, the aggregate is almost perfectly spherical and $K = 24$. When the flocs are substantially larger than the bubbles, the aggregate shape will approach the floc shape and $K = 45$. It is assumed here that K gradually varies from $K = 24$ at a floc size at or below 25 μm to $K = 45$ at a floc size at or above 100 μm.

Furthermore, aggregate rise rates are substantially higher than settling rates. As long as the flow regime remains laminar, which is characterized by a Reynolds number below unity, Equation (21) is valid. At higher rates, in the transition zone where Re = 1–50, the drag coefficient for particles with sphericity of 0.8 is estimated with (Brown 1963):

$$C_D = \frac{K}{Re^{0.75}} \tag{22}$$

In DAF applications, laminar flow is encountered below floc–bubble aggregate sizes of about 140–170 μm. Substitution of Equation (22) into Equation (14) allows estimation of the floc–bubble aggregate rise rate in the transition zone:

$$v_{fb} = \left(\frac{4}{3K}\right)^{0.8} \left(\frac{g^{0.8}(\rho_w - \rho_{fb})^{0.8} d_{fb}^{1.4}}{\rho_w^{0.2} \mu_w^{0.6}}\right) \tag{23}$$

Practical limits to *N*, the number of bubbles per floc

An important rise rate parameter is N, the number of bubbles that can be attached to each floc. There is a lower as well as an upper limit to N. The lower limit $N_{available}$ is determined by the number of available bubbles, which becomes a constraint when there are more flocs than bubbles (typically when the solids volume is distributed amongst numerous small flocs, such as at the onset of flocculation). The available surface area on the flocs determines the upper limit N_{max}.

With the number concentration of bubbles and flocs given by Equations (1) and (5), the number of available bubbles per floc (the lower limit of N) can be estimated by:

$$N_{available} = \left(\frac{C_b}{C_f}\right) \cdot \left(\frac{d_f}{d_b}\right)^3 \cdot \left[\left(\frac{\rho_w}{\rho_b}\right) + \left(\frac{\rho_p - \rho_w}{\rho_b}\right)\left(\frac{d_f}{d_p}\right)^{D_{fr}-3}\right] \tag{24}$$

Figure 10 shows the available number of bubbles per floc for a typical floc mass concentration of 5 mg l^{-1}, grown from primary clay particles only. Given the limited range of air dosing (average 8 mg l^{-1}) and bubble sizes (average 60 μm), the bubble concentration is relatively constant. The floc number concentration, however, is highly dependent on the degree of flocculation. The fractal dimension of the flocs has practically no influence; the numbers are

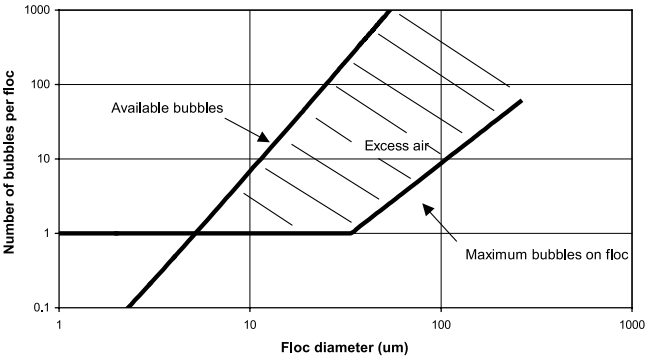

Figure 10 | Number of available and attachable bubbles for every floc as a function of floc diameter (conditions: C_f=5 mg l^{-1}, C_b=8 mg l^{-1}, d_b=60 μm, D_{fr}=2.2).

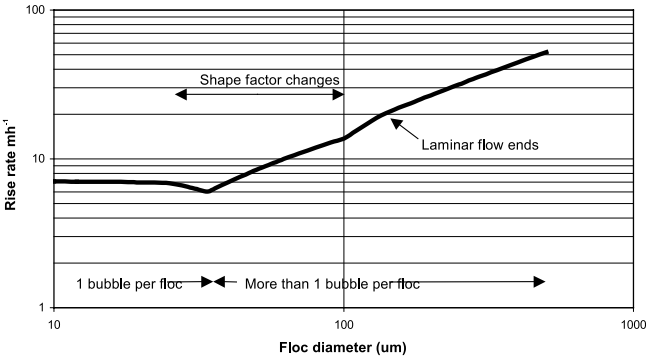

Figure 11 | Calculated rise rate for floc–bubble aggregates grown from kaolin primary particles, assuming maximum air efficiency and the densest possible bubble packing (conditions: C_f=5 mg l^{-1}, d_b=60 μm, D_{fr}=2.2, T=20°C).

solely a function of the solids concentration. For the floc mass concentration of 5 mg l^{-1} shown, the flocs only need to grow to about 5 μm to obtain approximately equal numbers of flocs and bubbles.

The upper limit of N is determined by the geometry of the bubbles and flocs. At least one bubble can be attached to a floc, even if a floc is much smaller than the bubble; an observation supported by photographic evidence (Ives 1995). It is also known that bubbles will not attach to flocs in layers (Tambo *et al.* 1986). For larger flocs, therefore, the surface area of the floc limits the number of bubbles that can be attached. The maximum number of bubbles attachable to a floc is estimated by assuming that each bubble occupies a square $d_b \times d_b$ on the floc surface (Tambo *et al.* 1986). This will provide a theoretical upper limit to N, despite the difficulty in visualizing such dense bubble packing:

$$N_{max}=\pi\left(\frac{d_f}{d_b}\right)^2 \tag{25}$$

Figure 10 shows the interplay between N_{max} and $N_{available}$. There are three regions to be considered. On the left, there are more small flocs than air bubbles. In the middle region, there are adequate bubbles to allow the attachment of one bubble to every floc with excess bubbles in suspension. In the region on the right, the available surface area of the floc controls the number of bubbles attached to every floc. Overall, we can see that the available number of bubbles per floc is critical when primary particles are small and flocculation times are short. Under these conditions, air efficiency (i.e. minimum loss of air to large bubbles due to coalescence), bubble size and air dosing concentration are critical. Once the floc has grown beyond say 10 μm, the number of bubbles per floc is decisively controlled by the constraints on bubble surface area. Even with the densest conceivable bubble packing shown assumed here, the available air is one to two orders higher than can be packed on to the floc. The fractal dimension of the floc plays no role. In reality the bubble size is not exactly 60 μm, but there are smaller and larger bubbles. Different bubble sizes slightly move the breakpoints in Figure 10, but the general conclusions remain the same.

The rise rate of the floc–bubble aggregate can now be predicted, taking into account the changing drag coefficient, Reynolds number, aggregate size and limitations of the number of attachable bubbles. The flocs are grown from primary particles only. The resulting rise rate for a typical case is shown in Figure 11, with the following comments:

- At small floc sizes, the rise rate is controlled by the bubble size. Bubble sizes different from 60 μm influence the rise rate in this regime.
- Increasing aggregate size above about 40 μm leads to a steady increase in rise rate.
- Rise rates obviously cannot increase indefinitely with aggregate size, as the possibility of bubble

detachment increases at the higher turbulence induced by higher rise rates.
- The analysis assumes flocs grown from primary clay particles only. When used with a precipitating coagulant, the additional precipitate will reduce the rise rate on the one hand, but the additional volume may add more opportunities for bubble attachment.
- If algae were the primary particles, there would be very little difference in the rise rate shown, as the rise rate is predominantly controlled by the buoyancy of the bubbles (compare the much higher rise rates in Figure 11 with the settling rates in Figure 9).

INSIGHTS GAINED FROM MODELLING

Contact zone modelling

The contact zone model shows that floc particles of 10s of microns have high η_T values and yield good contact zone removal efficiencies. Floc particles of 10s of microns should be prepared for the influent to DAF tanks. These theoretical predictions led Edzwald and co-workers (Edzwald *et al.* 1990; Edzwald 1995) to propose for drinking water treatment that flocculation tanks be designed differently for DAF clarification (i.e. tanks with smaller detention times and smaller size) than flocculation prior to sedimentation. Bench-scale studies (Edzwald & Wingler 1990) and pilot-scale studies (Edzwald *et al.* 1992; Valade *et al.* 1996; Edzwald *et al.* 1999) have demonstrated that good flotation performance can be achieved with flocculation times as low as 5–10 min. This contrasts with the work of others who have used flocculation-based collision models for the contact zone yielding predictions that large floc (>100 μm) should be formed for good flotation performance (Tambo *et al.* 1986; Fukushi *et al.* 1995, 1998; Leppinen 2000). However, pilot-scale data were shown in the Contact zone model confirmation section, confirming our approach of modelling the contact zone.

Contact zone modelling demonstrated the following points:

- Chemical pretreatment is vitally important. Optimum coagulation conditions of dose and pH that produce floc particles with little or no electrical charge yield flocs with favourable floc–bubble attachment. Flocculation detention times can be short since air bubbles in the contact zone collect particles and flocs of 10s of microns efficiently. However, mixing occurs in flocculation yielding a distribution of detention times and floc sizes. Particles of about 1 μm are not collected well by air bubbles in the contact zone.
- Bubble size and bubble volume concentration have a major impact on contact zone performance. Smaller bubbles improve the contact zone performance. Performance also improves with increasing air bubble volume concentrations. For contact zones with detention times exceeding 1.5 min and floc sizes 10–50 μm, performance is insensitive for bubble volume concentrations exceeding 6,000 ppm.
- The contact zone as traditionally defined should have a detention time of at least 1 min.
- The contact zone has been defined from the inlet up to the virtual boundary between what would *geometrically* be considered as the contact and separation zones. The *white water* actually extends beyond the baffle far into the separation zone. Clearly, there are additional opportunities for collisions and attachment of flocs to bubbles in this region, indicating that the contact zone should *operationally* be extended to include the entire *white water* zone.

Separation zone modelling

Separation zone modelling demonstrated the following points:

- The *floc structure*, which has a well-known and dramatic effect on the settling rate of flocs, has almost no effect on the rise rate of the typical floc–bubble aggregates found in dissolved flotation. The success of DAF is therefore not affected by the

floc structure, which is a marked departure from settling.

- The *bubble size* has a significant effect on rise rates. On the one hand, smaller bubble size leads to more bubbles which could be necessary to ensure a favourable bubble/floc number ratio when flocs are small and numerous. On the other hand, smaller bubbles lead to lower rise rates, which could be critical at higher hydraulic loadings. The calculated rise rate for 60 μm bubbles (Figure 11) is approximately double that for 40 μm bubbles. Although smaller bubbles could conceivably lead to more bubbles attaching to a floc, this effect is minor compared with the effect of bubble size.
- The *total air volume* is important when flocs are small and numerous, as it impinges upon the bubble/floc number ratio, provided the bubble sizes are unchanged. For large flocs, the total air volume is of negligible importance as there typically would be a large excess of air.
- Some flocculation is required to ensure floc sizes beyond about 10 μm. If this is not done and the bubble/floc number ratio is less than 1, an obviously unfavourable condition is reached. While the ratio can be improved by either increasing the air dosing or reducing the bubble size, the improvement will be limited within the normal ranges of air dosing and bubble size. The largest improvement is obtained by good flocculation, which will increase the floc size and reduce the floc number. The modelling shows that, for typical conditions, a minimum floc size of about 10 μm is required, which corresponds roughly to the guideline developed by Edzwald and co-workers (Edzwald *et al.* 1990; Edzwald *et al.* 1992) that flocs should be at least 10–30 μm for efficient collection by bubbles in the contact zone.
- If flocs are small or primary particles are present, it is further important to ensure optimal coagulation conditions. The situation here is that small particles or flocs have to be attached to a much larger bubble, which can clearly only happen under favourable surface charge conditions for both particles and bubbles. If the flocs are large, this could be of lesser importance as bubble enmeshment in the floc structure offers an additional attachment mechanism beyond simple point-to-point adhesion.

Models' shortcomings

The models presented in this paper necessarily include numerous simplifications and assumptions. Some of the most important shortcomings are:

- Bubbles and flocs are not uniform, but follow a distribution about a mean size.
- For both the contact zone and separation zone models, no allowances are made for bubble coalescence, particle growth by flocculation or the growth of floc–bubble aggregates.

Furthermore, the complex hydrodynamic flow patterns in both the contact and separation zones were not accounted for in the models presented. The usual approach is to ignore these complications, which implies the following assumptions:

- Plug flow is explicitly assumed to calculate the efficiency of the contact zone, as was also done in the contact zone model presented here. The deviations from plug flow in the contact zone need to be characterized and the model refined to take this into account. The fact that experimental data (Figure 8) supported the plug flow contact zone model with reasonable assumptions, indicates that the deviations from plug flow may not be too severe, but it remains to be investigated.
- If the flow through the separation zone moved as a perfect plug from inlet to outlet, one could argue that the maximum hydraulic loading should only be less or equal to the aggregate rise rate to obtain perfect aggregate separation. This assumption of plug flow is indeed found in most publications, arguing that the time for aggregate to rise to the top of the tank only needs to be less than the time taken for the water to reach the separation zone outlet. If the deviations from plug flow, however, were significant, then the relationship between hydraulic

loading and rise rate becomes complex and requires more attention.

The last two assumptions are both idealistic and are considered in the next section.

HYDRODYNAMIC CONSIDERATIONS

Dealing with deviations from plug flow

Plug flow conditions, as often assumed in process engineering, rarely exists. A common way to account for practical deviations from plug flow is to assume an axial dispersion coefficient D. The spreading rate for a liquid as it moves through a tank or vessel can then be quantified by the *dispersion number* D_{sp}, which would be characteristic for a specific tank:

$$D_{sp}=\frac{D}{VL} \tag{26}$$

In the DAF literature (for example, Baeyens *et al.* 1995; Shawwa & Smith 1998) the inverse of the dispersion number is commonly referred to as the Peclet number. Levenspiel (1989), however, points out that the Peclet number should only be used when the longitudinal transfer is due to molecular diffusion, and not when it is due to dispersion (which also includes the effects of velocity gradients, turbulent eddies and dead volume fraction m). Thus, we appropriately use the dispersion number.

An analysis of large, shallow, rectangular outdoor basins (Thackston *et al.* 1987) did identify the length/width ratio to have the strongest influence on the dispersion number (compared with wind and depth), but failed to derive a reliable predictive relationship for the dispersion number. Other studies (summarized by Baeyens *et al.* 1995), however, did report some general relationships for tanks with free surfaces. For rectangular tanks:

$$D_{sp}=[0.5+1.4(L/W)]^{-1} \tag{27}$$

$$m=1-0.9(1-e^{-0.4L/W}) \tag{28}$$

The length L is defined in the flow direction, and the width W measured from side to side. If the dispersion number is 0.05 or lower, plug flow can be assumed for practical purposes (Baeyens *et al.* 1995). According to Equation (27), this could be reached at L/W ratios of 14 or more. The corresponding dead volume fraction is 10%.

Contact zone hydrodynamics

Baeyens *et al.* (1995) and Shawwa & Smith (1998) conducted tracer tests in laboratory-scale contact zones, configured as cylindrical columns with length/diameter ratios of more than 10, an arrangement known to favour plug flow conditions. From their work, useful findings followed:

- The axial dispersion model, with open-open boundary conditions, described the degree of mixing within the contact zone reasonably well. (Open-open boundary conditions assume an undisturbed flow pattern at both the inlet and outlet of the reactor. This is considered to be an adequate approximation despite the small jets formed by some types of injection nozzles.)
- The introduction of 10% recycle increased the dispersion number by 10% to 20% in comparison with the case with no air.
- At a typical hydraulic loading of 70 m h^{-1} with about 10% recycle, the dispersion numbers measured in the two studies were about 0.01 and 0.03, respectively.

For these optimal laboratory configurations, the hydrodynamical conditions were therefore very close to plug flow, even after the introduction of the air suspension. In a conventional full-scale contact zone, the flow is upward and there is no free surface parallel to the flow direction. The typical flow length is about 3 m (equal to the depth of the DAF reactor), and the effective width is typically about 1 m (the average distance between the inlet wall and the baffle), as depicted in Figure 12. If these values are used in Equation (27), a dispersion number of about 0.2 is obtained. (In reality, the dispersion number will be lower, due to the absence of a free surface parallel to the flow

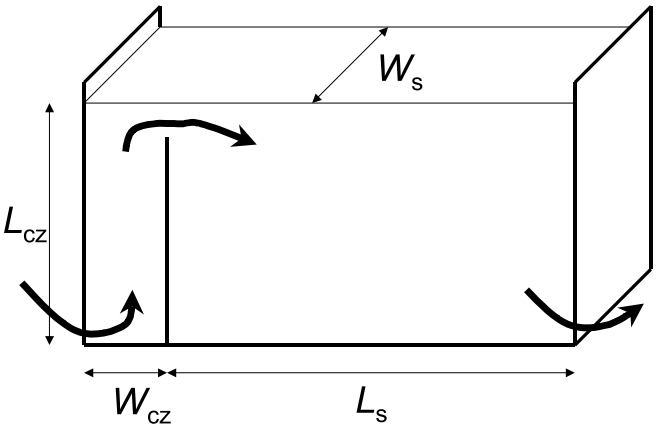

Figure 12 | Assignment of length L and width W to the contact and separation zones.

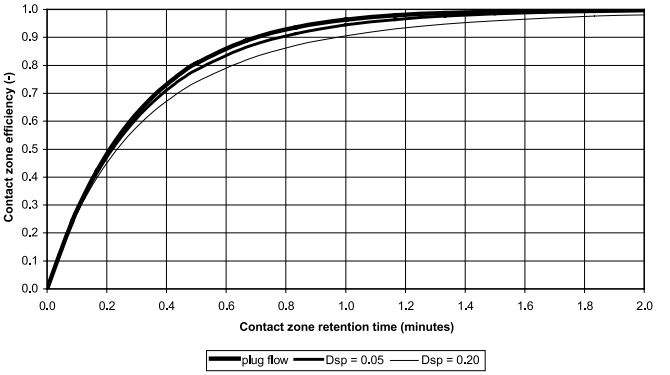

Figure 13 | Effect of axial dispersion on the contact zone efficiency (conditions: d_b=60 μm, μ_{fb}=0.5, d_f=30 μm, φ_b=6,000 ppm, T=293 K, D_{sp}=0.05 and 0.2).

direction.) To illustrate the worst scenario, a very high dispersion number 0.2 is used in the next section.

Contact zone efficiency

How would this deviation from plug flow impact on the contact zone efficiency? The removal rate of particles or flocs in the contact zone was presented as Equation (6). The DAF removal rate coefficient (Equation (7)) yields the following form after substituting for A_b ($\pi d_b^2/4$), for n_b using Equations (1) and (2), and using Equation (21) to describe the rise rate (v_b) of bubbles for laminar flow and assuming the bubble density is negligible compared with the water density.

$$k_c=\frac{\alpha_{fb}\eta_T d_b \psi_b g p_w}{12\mu_w} \tag{29}$$

For a reactor with open-open boundary conditions, the following removal efficiency equation was reported by Baeyens *et al.* (1995):

$$X=1-\frac{4\beta}{(1+\beta)^2 e^{-0.5(1-\beta)/D_{sp}}-(1-\beta)^2 e^{-0.5(+\beta)/D_{sp}}} \tag{30}$$

with the parameter β defined by:

$$\beta=\sqrt{1+4k_c t_{cz} D_{sp}} \tag{31}$$

Figure 13 shows the effect of dispersion number on the removal efficiency of a typical DAF contact zone, from which follows:

- Dispersion within the contact zone has a very small effect on the contact zone efficiency, even at a high dispersion number of 0.2.
- Further analysis (not shown) shows that the effect of dispersion remains very small over the full range of practical temperatures, bubble sizes, floc sizes and attachment efficiencies.
- Contact zone efficiency is therefore a primary function of the factors identified in the earlier section on contact zone modelling. The refinements brought about by a better description of the hydrodynamic conditions have negligible effect.

Separation zone hydrodynamics

The geometrical L/W ratio in a typical DAF separation zone would be 4 or less if based on L the horizontal length and W the width of the separation zone (see Figure 12). It could be argued that the mean flow pattern does not only follow a horizontal plane from left to right, but also a vertical plane from top (at the inlet) to bottom (at the withdrawal point), and that the mean flow path should be

slightly more than the horizontal length. In some DAF tanks, the withdrawal is made along the length of the tank floor, and not only at the far bottom end. As we are dealing here with approximate estimates of the hydrodynamic characteristics of the separation zone, these marginal refinements are unnecessary. If the flow of *water only* is considered, Equation (27) indicates a dispersion number of 0.17 or more. If air *is added to the water*, the matter is significantly complicated:

- If the water flows co-currently upwards with the rising direction of the air bubbles, the presence of the air increases the dispersion number by 10% to 20%, as was pointed out in the previous section on co-current contact zones.
- In a conventional DAF separation zone, the bubbles rise perpendicularly to the general flow direction, which should cause greater dispersion.
- The flow pattern is further distorted by the high-density gradients induced by the air suspension. Unlike the contact zone, where the air concentration is relatively constant throughout, the separation zone has an upper region where air is concentrated, and a lower region where the water is practically devoid of air. A much higher degree of dispersion is expected in this case, and it is intuitively clear that the actual flow pattern in the separation zone deviates significantly from plug flow.

A better understanding of separation zone hydrodynamics followed from the work of Lundh & Jonsson (2002*b*). A series of pulse tracer tests were performed with dilute suspensions (less than 30 mg SS l^{-1}) of biological effluent on a pilot plant with a small separation zone (0.7 m wide, 1.33 m long and 1.25 m deep) with the hydraulic loading rate and recycle rate as the main variables. Without recycle, the tracer pulse in the effluent peaked at about half the theoretical detention time with a long period following to wash out the tail of the tracer pulse. This indicates a circular mixing pattern in the separation zone, approaching that of a completely mixed reactor. With recycle at typical rates, the tracer response was very different. The tracer pulse showed a sharp peak very close to the theoretical detention time, with fairly quick washout of the tracer tail. When low recycle rates were used together with high hydraulic loading rates, the peak retained its position at the theoretical detention time but flattened with a longer washout tail.

The tracer tests described were supplemented with direct measurements of flow velocity using ADV (acoustic Doppler velocimetry) (Lundh *et al.* 2001; Lundh & Jonsson 2002*a*). A consistent pattern was observed. When typical recycle and loading rates were used, a strong horizontal current on the surface towards the far wall was measured, with a horizontal return current immediately below (a condition termed as a 'stratified' condition). When either the hydraulic loading rate was increased, and/or the recycle rate was decreased (in other words when the air/water ratio was lowered), the forward horizontal current was drawn below the surface towards the outlet with a much more haphazard return current (termed a 'short-circuit' condition). The air concentration in the lower parts of the separation zone was much greater during the short-circuit condition. For the experimental system tested, an air concentration of 8 mg l^{-1} was sufficient to sustain stratified conditions for hydraulic loading as high as 25 m h^{-1}. At a hydraulic loading of 18 m h^{-1}, an air concentration of 6 mg l^{-1} was required for stratified conditions; at 12 m h^{-1} an air concentration of 3 mg l^{-1} was sufficient.

This phenomenon is, broadly speaking, confirmed by a recent study measuring the flow patterns in a small separation zone (0.30 m wide, 0.50 m long by 0.35 m deep) with LDV (laser Doppler velocimetry), a technique less intrusive than ADV (Hague *et al.* 2002). Without air, the flow pattern was completely mixed. When very small air concentrations were added (as low as 0.6% recycle rate), the flow pattern changed from completely mixed to a stratified structure.

Another approach to unravel the intricate hydrodynamics of the separation zone is the use of computational fluid dynamics (CFD). Such CFD studies have demonstrated patterns broadly resembling the experimental work reported above (for example Fawcett 1997; Crossley *et al.* 2000; Hague *et al.* 2002). In principle, CFD is a powerful tool which can predict the flow pattern and the air concentration at all points in the separation zone.

However, the CFD studies published up to now lack convincing, vigorous benchmarking and validation for DAF applications. Due to the problems inherent in measuring velocity in a reactor obscured by bubbles, without interfering with the flow pattern, it has understandably seldom been attempted. In a rare case where simultaneous modelling and measurement were performed (Hague *et al.* 2002), reasonably good agreement between modelling and measurement of velocity was found, but the agreement between measured and predicted air concentration was less convincing. Due to the measuring difficulties, practical measurements had to be confined to such small reactors that the findings cannot yet be generalized to full-scale DAF tanks.

The CFD studies have all ignored the presence of particles and the effects of coagulation; two-phase flow of discrete bubbles and water only are modelled. The second author, however, observed a clearly discernible effect on the flow pattern in a pilot plant in treating a reservoir water supply with and without the use of coagulant. As soon as coagulant was added, the *white water* blanket stabilized at a higher position in the separation zone. Without coagulant addition, the blanket was drawn deeper into the tank and closer to the outlet. Whether this was a surface charge, or a particle-induced phenomenon, was not clear. This observation was supported by the experimental work of Lundh *et al.* (2002) in treating wastewater. A few tests were conducted with SS concentrations varying from 0 mg l^{-1} (tap water) to as high as 102 mg l^{-1}. It was found that particle removal was *better* at high SS concentration, all other conditions being the same. The high SS concentration seemed to improve the flow structure from short-circuit flow towards stratified flow, but no mechanistic explanation could be put forward for this finding.

Although we are still far away from a reasonably complete understanding of separation zone hydrodynamics, the following preliminary conclusions are made:

- The geometry of a typical rectangular DAF separation zone is such that if water alone were to flow through it, significant deviations from plug flow are probable.
- The presence of air bubbles in the water leads to a complete change in flow pattern, which can be ascribed to large density gradients induced by the air bubbles.
- At typical DAF recycle and hydraulic loading rates, a stratified flow structure is observed where a horizontal surface current towards the outlet wall is accompanied by a reverse current immediately below, with a steep hydraulic gradient between the currents.
- Should the hydraulic loading rate be increased and/or the recycle rate decreased, a short-circuit flow structure is approached, characterized by a lowering of the outward current towards the outlet wall, an increased air content in the lower parts of the separation zone and reduced particle removal.
- There is evidence that the addition of coagulant and/or high SS concentrations may reinforce a stratified flow structure with better particle removal.

EVOLUTION OF HYDRAULIC LOADING RATES FOR DAF

It was shown in the previous section that the simplistic approach of a floc–bubble aggregate steadily rising to the surface as the entire body of fluid is steadily moving through the tank is untenable because of the complex hydrodynamical flow structure within the separation zone. In this section, the evolution of hydraulic loading rates in practice is compared with the theoretical rise rates modelled in this paper and shown in Figure 11.

Historically, DAF tanks were designed in Europe, South Africa and the USA at loadings of 2.5–15 m h^{-1}. Most of the plants built in the late 1960s through the 1980s were designed with fairly conservative loadings of 4–10 m h^{-1}. These plants also had fairly long flocculation times, similar to that required for settling. This was due to implementation of a new technology to potable water treatment and in some cases because of incorporating DAF above the granular media filter. The plants, especially

outside the USA, were used widely to treat mesotrophic or eutrophic supplies high in algae and supplies high in natural colour. In the USA, there has been some application of DAF in treating supplies high in colour; however, most applications have been in treating low turbidity, oligotrophic reservoirs.

Since about 1990, several plants in the USA have been designed at 15 m h^{-1} (Nickols & Crossley 1997). One of these plants has been in operation for 3 years and is a 190 Ml day^{-1} plant in Fairfield, Connecticut, with a relatively short flocculation time of 12 min. Coagulation is optimized at this plant and pH is controlled in the mid 6s producing favourable conditions for bubble–particle attachment; consequently, the performance is very good, with DAF turbidities generally 0.3–0.5 NTU. Even when the water temperature is 1–4°C, the plant produces DAF turbidities of 0.5–1 NTU. Extensive pilot plant studies for designs of plants for Boston (1,500 Ml day^{-1}) and New York City (1,100 Ml day^{-1}) have demonstrated good performance at higher DAF loadings of 15–20 m h^{-1} and flocculation times of 5–10 min. Edzwald *et al.* (1999) showed, through extensive pilot studies at two sites in the USA, that DAF plants can perform well with a short flocculation time of 5 min, hydraulic loadings of 20–40 m h^{-1} and a filtration rate of 20 m h^{-1}. Air bubbles were drawn into the outlet of DAF separation zones at loadings of about 20 m h^{-1} or greater, but these bubbles were not associated with particles. The excess air bubbles could be removed ahead of the filters or allowed to carry to the filters. In the latter case, the bubbles rose to the surface in the water above the filters with no detrimental impact on filtration. A DAF plant is now in operation in Tampere (Finland) treating high quality lake water, which was designed at a hydraulic loading of nearly 40 m h^{-1} (Kiuru 2000).

The trend in the USA then is to decrease flocculation times and to increase DAF loadings. This means that small floc particles (10s of μm) can be removed at high DAF loadings and contradicts the conventional wisdom that large floc and aggregates of flocs and bubbles are needed for successful separation. It should be pointed out that in most of the USA applications, coagulation and pH conditions were optimized leading to favourable conditions for bubble–particle attachment.

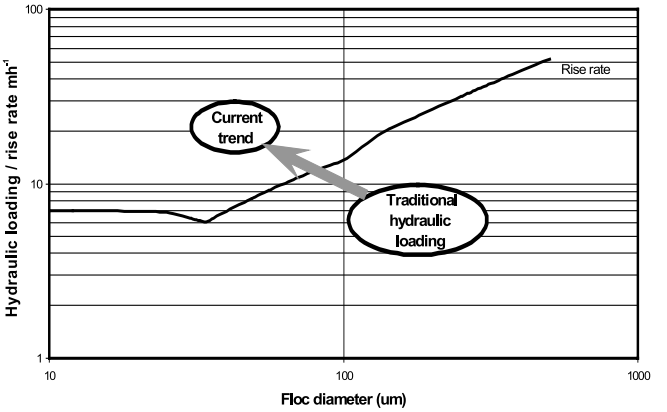

Figure 14 | Evolution of DAF design parameters from the 1970s to the 1990s in comparison with theoretical floc–bubble rise rates presented in Figure 11.

Figure 14 shows the theoretical rise rates reported earlier, this time together with the general regions at which DAF systems were traditionally designed and operated, and where the last decade of experimentation and implementation has been leading us. The simplistic plug-flow view of the separation zone is therefore clearly ruled out by the hydraulic loading rates at which recent DAF applications have been shown to work well. This echoes the conclusion made earlier on the strength of measured and modelled hydrodynamic flow patterns. Does successful DAF require that the aggregate rise rate *has* to be larger than the hydraulic loading rate to prevent the aggregates from being drawn into the outlet with the effluent? Using the well-known argument that theoretical aggregate removal from either settling or DAF tanks does not depend on tank depth, but only on the surface loading, it is argued that the stratified flow structure effectively produces two stacked linear-flow reactors, one leading the flow on the surface from the inlet to the far end and the other returning the flow below the surface. This effectively doubles the separation zone surface area for flotation so the hydraulic loading can be about twice that based on the physical footprint surface area. Even allowing for this phenomenon, as well as the approximations made for the estimation of the aggregate rise rate, it seems convincing that practical loading rates are now beyond what can be theoretically explained.

SUMMARY, CONCLUSIONS AND FUTURE DIRECTIONS

The development of DAF modelling, up to now, had been done in a piecemeal fashion. The process was conveniently separated into a contact step and a separation step; each with its own idealized flow patterns. Despite these inherent limitations, the models presented in the above sections have served their purpose admirably well. They also serve as valuable stepping-stones towards more comprehensive modelling in the future. The model for the contact zone illustrated the following important requirements for efficient DAF:

- Optimal chemical (coagulation) pretreatment and flocculation are vitally important to reach acceptable attachment efficiency between bubbles and flocs.
- Primary particles or flocs should be about 10 μm or greater in size to be collected by bubbles in the contact zone.
- Bubble size has a major impact on contact zone efficiency; smaller bubbles improve contact zone performance.
- It is important to have an adequate bubble volume concentration. Once floc–bubble aggregate sizes of 10–50 μm are reached and the contact time exceeds 1.5 min, performance is insensitive to bubble volumes exceeding 6,000 ppm.
- The contact zone requires a mean detention time of at least 1 min.

The actual flow pattern in the conventional contact zone (which is the vertically rising section up to the top of the baffle separating the contact zone from the separation zone) does not deviate much from ideal plug flow. Even if these deviations are taken into account, they have a very minor impact on the contact zone efficiency. In this respect, the idealized contact zone model presented cannot be much improved by sophisticated hydrodynamic refinements.

The theoretical estimate of the floc–bubble aggregate rise rate, in turn, also established some important conditions for efficient separation by DAF:

- DAF is practically insensitive to floc structure compared with settling, because the buoyancy is almost exclusively determined by the attached air and not by the mass of the flocs.
- The importance of bubble size is explicitly shown; smaller bubbles distribute the available air over *more* bubbles, but larger bubbles lead to higher *rise rates*.
- The benefits of larger flocs are twofold: the floc number concentration is dramatically reduced as flocs grow, making more air available for each floc (at all floc sizes), and the available surface for bubble attachment increases (at floc sizes beyond about 50 μm). These advantages are partly offset by the larger probability that bubbles may be sheared from the larger, more rapidly rising floc–bubble aggregates, a complex phenomenon not considered in this paper.
- Provided that flocs grow in excess of 30 μm, the total air volume plays no role, as there is a large excess of air in the suspension.

The hydrodynamics of the separation zone are complex and poorly understood, but the following findings have recently emerged:

- Under ideal conditions of adequate air and average hydraulic loading, a *stratified* flow structure is found, which is distinguished by a horizontal current on or close to the surface, running from the inlet towards the outlet wall. A return current towards the inlet is formed immediately below, which sets up a significant velocity gradient in the top of the tank. From the top layers, there is a relatively uniform vertical flow down towards the outlet.
- When the air is reduced, and/or the hydraulic loading rate is increased beyond certain thresholds, the stratified flow structure breaks down and a *short-circuited* flow structure forms. This is characterized by the downward deflection of the horizontal current towards the outlet, with a poorly defined and seemingly haphazard return current.
- Short-circuited flow is accompanied by a higher air content in the bottom of the separation zone, and also by poorer removal of incoming aggregates.

- The threshold between stratified and short-circuit flow is also influenced by the addition of coagulants and the solids concentration.

What then are the weaknesses of the models presented for the contact and separation zones? The most glaring overall weakness is their inability to explain the very high loading rates implemented at new DAF plants during the past decade. This can be broken down into a number of questionable assumptions:

- Bubbles, floc particles and aggregates do not all have the same size, but are all distributed about a mean. More advanced modelling may eventually include *distributions* rather than just average sizes, but this refinement is not expected to yield dramatically different conclusions.
- The models consider the sizes of bubbles, flocs and aggregates to be fixed once contact between bubbles and flocs has been established. While this approach will yield a reliable snapshot of conditions *at the start of the contact zone*, it will obviously fail to account for further bubble coalescence, flocculation of particles and growth of aggregates. As these processes most probably remain at work, the models will therefore not give a reliable prediction of conditions *at the end of the separation zone*, which is the primary objective.
- No allowance is made for detachment or shear of the aggregates. The importance of this phenomenon is known from two-phase flocculation modelling, and there is no reason why it should not be equally important in the DAF three-phase system.
- The stratified flow in the separation zone can provide a simple explanation of why DAF tanks can operate at higher hydraulic loadings compared with theoretical rise rates of bubble–particle aggregates. Stratified flow can be simplistically visualized as two vertically stacked tanks with a combined surface area double that of the footprint of the separation zone, leading to improved separation efficiency.

What are likely to be the most profitable areas of future DAF modelling efforts?

- The traditional boundary between the contact and separation zones has been one of geometrical convenience with little regard for what is going on within the suspension. The interaction between flocs, bubbles and aggregates will continue wherever they exist in close proximity. The contact zone should then be extended to include the entire *white water* region. The contact zone would therefore have two parts: the traditional vertical section, with relatively simple hydrodynamics, and the top part of the traditional separation zone, with very complex hydrodynamics. The collision, attachment and detachment rates in these two parts will be different, and pose significant challenges for future modelling efforts.
- Consideration of the underside of the float layer in the separation zone as an additional collector surface for the aggregates suspended in the top layer of the stratified flow structure, especially in the region where the upward flow from the contact zone changes direction towards the separation zone outlet.
- The promising contributions made up to now by CFD will have to be extended to deal with collision, attachment and detachment rates as outlined above. By assuming static distributions of bubbles and neglecting the particulate part of the suspension, as almost all efforts up to now have done, CFD loses much of the realism of DAF and contributes little more than the models developed in this paper.
- A proper and predictive understanding of the hydraulic behaviour of the traditional separation zone, with better characterization of what is now loosely defined as stratified and short-circuited flow structures, is essential to be able to estimate the velocity gradients within, which is probably the primary mechanism through which continued floc–bubble interaction takes place.

Resolution of these areas, and their integration into a comprehensive DAF model, should not only bring better convergence between theory and practice, but also point out directions for optimization of the DAF process.

ACKNOWLEDGEMENTS

The authors thank Charles R. O'Melia and John E. Tobiason for constructive comments they provided on a draft of the paper. The authors are also greatly appreciative to former students for their many contributions on DAF and the knowledge they imparted to us. Without their efforts, this paper would not be possible. Over the years, the authors have benefited from numerous collaborations with colleagues in consulting, water utilities and process equipment organizations. We thank them for their assistance.

LIST OF SYMBOLS

A	area in plan
C	mass concentration
C_D	drag coefficient
d	size or diameter
dH	differential reactor depth
D	axial dispersion coefficient
D_{fr}	fractal dimension
D_{sp}	dispersion number
g	gravitational constant of acceleration
k_b	Boltzmann's constant
k_c	first-order floc or particle removal rate constant
K	shape factor
L	reactor length
m	dead volume fraction
n	number concentration
N	number of bubbles per floc
Re	Reynolds number
v	settling or rise rate
V	average flowthrough velocity
t	detention time
T	absolute temperature
W	reactor width
α	attachment efficiency factor
β	intermediate parameter
ϕ_b	bubble volume concentration
η	single collector efficiency
μ	dynamic viscosity
ρ	density
subscript b	indicating *bubble*
subscript cz	indicating *contact zone*
subscript D	indicating *Brownian diffusion*
subscript e	indicating *effluent*
subscript f	indicating *floc*
subscript fb	indicating *floc–bubble*
subscript i	indicating *influent*
subscript I	indicating *interception*
subscript IN	indicating *inertia*
subscript p	indicating *primary particle*
subscript pb	indicating *particle–bubble*
subscript S	indicating *settling*
subscript T	indicating *total*
subscript w	indicating *water*

REFERENCES

Adachi, Y. & Tanaka, Y. 1997 Settling velocity of an aluminium-kaolinite floc. *Wat. Res.* **31**(3), 449–454.

Amato, T., Edzwald, J. K., Tobiason, J. E., Dahlquist, J. & Hedberg, T. 2001 An integrated approach to dissolved air flotation. *Wat. Sci. Technol.* **43**(8), 19–26.

Baeyens, J., Mochtar, I. Y., Liers, S. & De Wit, H. 1995 Plugflow dissolved air flotation. *Wat. Environ. Res.* **67**(7), 1027–1035.

Brown, G. G. 1963 *Unit Operations*. John Wiley & Sons, New York.

Crossley, I. A., Valade, M. T. & Shawcross, J. 2000 Using lessons learned and advanced methods to design a 1,500 ML/day DAF water treatment plant. *Wat. Sci. Technol.* **43**(8), 35–41.

Derjaguin, B. V., Dukhin, S. S. & Rulyov, N. N. 1984 Kinetic theory of flotation of small particles. In *Colloid and Surface Science* (ed. Matijevic, E. & Good, R. J.), vol. 13, pp. 71–113. Plenum Press, New York.

Edzwald, J. K. 1995 Principles and applications of dissolved air flotation. *Wat. Sci. & Technol.* **31**(3–4), 1–23.

Edzwald, J. K. & Wingler, B. J. 1990 Chemical and physical aspects of dissolved-air-flotation for the removal of algae. *J. Wat. Suppl.: Res. & Technol.–AQUA* **39**(1), 24–35.

Edzwald, J. K., Malley, J. P. & Yu, C. 1990 A conceptual model for dissolved air flotation in water treatment. *Wat. Suppl.* **8,** 141–150.

Edzwald, J. K., Walsh, J. P., Kaminsky, G. S. & Dunn, H. J. 1992 Flocculation and air requirements for dissolved air flotation. *J. Am. Wat. Wks Assoc.* **84**(3), 92–100.

Edzwald, J. K., Tobiason, J. E., Amato, T. & Maggi, L. J. 1999 Integrating high rate dissolved air flotation technology into plant design *J. Am. Wat. Wks Assoc.* **91**(12), 41–53.

Fawcett, N. S. J. 1997 The hydraulics of flotation tanks: computational modeling. Paper presented at the *International Conference on Dissolved Air Flotation, London, April 1997*.

Fukushi, K., Tambo, N. & Matsui, Y. 1995 A kinetic model for dissolved air flotation in water and wastewater treatment. *Wat. Sci. & Technol.* **31**(3-4), 37–48.

Fukushi, K., Matsui, Y. & Tambo, N. 1998 Dissolved air flotation: experiments and kinetic analysis. *J. Wat. Suppl.: Res. & Technol.–AQUA* **47**(2), 76–86.

Gregory, J. 1989 Fundamentals of flocculation. *Critical Rev. Environ. Control* **19**(3), 185–249.

Haarhoff, J. & Edzwald, J. K. 2001 Modelling of floc–bubble aggregate rise rates in dissolved air flotation. *Wat. Sci. & Technol.* **43**(8), 175–184.

Haarhoff, J. & Steinbach, S. 1997*a* Towards the maximal utilization of air in dissolved air flotation. *Proceedings of an International Conference, Dissolved Air Flotation, April 1997*. Chartered Institution of Water and Environmental Management, pp. 25–34.

Haarhoff, J. & Steinbach, S. 1997*b* A comprehensive method for measuring the air transfer efficiency of pressure saturators. *Wat. Res.* **31**(5), 981–990.

Haarhoff, J. & Van Vuuren, L. 1993 *A South African Design Guide for Dissolved Air Flotation*. Water Research Commission, Pretoria, South Africa.

Hague, J., Ta, C. T. & Biggs, M. J. 2002 Experimental and modelling study of flow in DAF tanks. Submitted to *Wat. Res.*

Han, M. Y. 2000 Modelling of DAF: the effect of particle and bubble characteristics. Paper presented at an *IWA Workshop on the Modelling of Conventional Drinking Water Production Processes, Delft, March 2000*.

Han, M. Y., Park, Y. H. & Yu, T. J. 2002 Development of a new method of measuring bubble size. *Wat. Sci. & Technol.: Wat. Suppl.* **2**(2), 77–83.

Ives, K. J. 1995 Inside story of water treatment processes. *J. Environ. Engng, ASCE* **121**(5), 846–849.

Jiang, Q. & Logan, B. E. 1991 Fractal dimensions of aggregates determined from steady-state size distributions. *Environ. Sci. Technol.* **25**(12), 2031–2038.

Johnson, C. P., Li, X. & Logan, B. E. 1996 Settling velocities of fractal aggregates. *Environ. Sci. Technol.* **30**(6), 1911–1918.

Kiuru, H. J. 2000 Development of dissolved air flotation technology from the 1st generation to the newest or 3rd one. *Proceedings of the 4th International Conference on Dissolved Air Flotation in Water and Waste water Treatment, Helsinki*.

Leppinen, D. M. 2000 A kinetic model of dissolved air flotation including the effects of interparticle forces. *J. Wat. Suppl.: Res. & Technol. AQUA* **49**(5), 259–268.

Levenspiel, O. 1989 *The Chemical Reactor Omnibook*. Oregon State University Bookstores, Inc., Corvallis, Oregon.

Liers, S., Baeyens, J. & Mochtar, I. 1996 Modeling dissolved air flotation. *Wat. Environ. Res.* **68**(6), 1061–1075.

Logan, B. E. & Kilps, J. R. 1995 Fractal dimensions of aggregates formed in different fluid mechanical environments. *Wat. Res.* **29**(2), 443–453.

Lundh, M. & Jonsson, L. 2002*a* Performance evaluation of the acoustical Doppler velocimeter in water with high contents of micro-bubbles. Paper B of a doctoral dissertation Effects of Flow Structure on Partical Separation in Dissolved Air Flotation, submitted to Lund University, Sweden.

Lundh, M. & Jonsson, L. 2002*b* RTD characterization of the flow structure in dissolved air flotation. Paper H of a doctoral dissertation Effects of Flow Structure on Partical Separation in Dissolved Air Flotation, submitted to Lund University, Sweden.

Lundh, M., Jonsson, L. & Dahlquist, J. 2001 The flow structure in a separation zone of a DAF pilot plant and the relation with bubble concentration. *Wat. Sci. & Technol.* **43**(8), 185–194.

Lundh, M., Jonsson, L. & Dahlquist, J. 2002 Relating the separation of biological floc from the Kaldnes moving bed biobed process to the flow structure in a dissolved air flotation pilot tank. Paper G of a doctoral dissertation Effects of Flow Structure on Partical Separation in Dissolved Air Flotation, submitted to Lund University, Sweden.

Malley, J. P. Jr & Edzwald, J. K. 1991 Concepts for dissolved air flotation treatment of drinking waters. *J. Wat. Suppl.: Res. & Technol.–AQUA* **40**(1), 7–17.

Nickols, D. & Crossley, I. A. 1997 The current status of dissolved air flotation in the USA, paper presented at the *International Conference on Dissolved Air Flotation, London, April 1997*.

Rykaart, E. M. 1994 Die Verfyning van Inspuitnossels vir Opgelostelugflottasie. (The refinement of air injection nozzles for dissolved air flotation.) MEng dissertation, Rand Afrikaans University, Johannesburg, South Africa.

Schers, G. J. & Van Dijk, J. C. 1992 Dissolved-air flotation: theory and practice. In *Chemical Water and Wastewater Treatment II* (ed. Klute, R. & Hahn, H. H.), pp. 223–246. Springer Verlag, New York.

Shawwa, A. R. & Smith, D. W. 1998 Hydrodynamic characterization in dissolved air flotation (DAF) contact zone. *Wat. Sci. & Technol.* **38**(6), 245–252.

Tambo, N. & Watanabe, Y. 1979 Physical characteristics of flocs–I. The floc density function and aluminium floc. *Wat. Res.* **13**(5), 409–419.

Tambo, N., Matsui, Y. & Fukushi, K. 1986 A kinetic study of dissolved air flotation. *World Congress of Chemical Engineering, Tokyo, 1986*.

Thackston, E. L., Shields, F. D. & Schroeder, P. P. 1987 Residence time distributions of shallow basins. *J. Environ. Engng, ASCE* **113**(6), 1319–1331.

Valade, M. T., Edzwald, J. K., Tobiason, J. E., Dahlquist, J., Hedberg, T. & Amato, T. 1996 Particle removal by flotation and filtration: pretreatment effects. *J. Am. Wat. Wks Assoc.* **88**(12), 35–47.

Wiesner, M. R. 1992 Kinetics of aggregate formation in rapid mix. *Wat. Res.* **26**(3), 379–387.

Yao, K. M. 1968 Influence of Suspended Particle Size on the Transport Aspect of Water Filtration. PhD dissertation, University of North Carolina, Chapel Hill, North Carolina.

Yu, T. 1989 Modeling of Dissolved Air Flotation for Drinking Water Treatment. MS thesis, University of Massachusetts, Amherst, Massachusetts.

First received 30 January 2003; accepted in revised form 23 September 2003